Supporting Information

Enhancing Electrical and Optoelectronic Properties of ZnO via Interfacial Charge Transfer with Strong Electron Donors

Yi-Lin Gao, [abc] Wen-Yan Xu, [abc] Fei-Ping Lai, [bd] Hong-Zhi Xiao, [abc] Shu-Juan Lin,[*b] Li-Zhen Cai,[*b] Kai-Bin Jiang, [bd] De-Lin Hu, [bd] Ming-Sheng Wang,[*b] and Guo-Cong Guo[*b]

[a]College of Chemistry, Fuzhou University, Fuzhou, Fujian 350108, P. R. (China)

[b]State Key Laboratory of Structural Chemistry, Fujian Institute of Research on the Structure of Matter, Chinese Academy of Sciences, Fuzhou, Fujian 350108 (China)

[c]Fujian College, University of Chinese Academy of Sciences

[d]University of Chinese Academy of Sciences, Beijing, P. R. (China)

E-mail: sjlin@fjirsm.ac.cn (S.-J. Lin); clz@fjirsm.ac.cn (L.-Z. Cai); mswang@fjirsm.ac.cn (M.-S. Wang); gcguo@fjirsm.ac.cn (G.-C. Guo)

Experimental details

Characterization. A series of structural and spectroscopic techniques were employed to characterize the samples. The crystal structures were analyzed by powder X-ray diffraction (PXRD) using a Rigaku SmartLab MiniFlex II diffractometer (Japan) with Cu K_α radiation (λ = 1.5406 Å). Surface morphologies were examined on a Zeiss Sigma 300 field-emission scanning electron microscope (SEM) operated at an accelerating voltage of 10 kV. .Detailed microstructural information, including transmission electron microscopy (TEM), high-angle annular dark-field scanning TEM (HAADF-STEM), and elemental mapping, was obtained using an FEI Talos F200S G2 microscope operated at 200 kV. X-ray Photoelectron Spectroscopy (XPS) and Ultraviolet Photoelectron Spectroscopy (UPS) were performed on an ESCALAB 250Xi spectrometer (Thermo Fisher Scientific) using monochromatic Al Kα radiation ($h\nu$ = 1486.6 eV). All binding energies were calibrated with respect to the adventitious C 1*s* peak at 284.8 eV. UV–vis spectra were recorded with a PerkinElmer Lambda 950 UV/vis/NIR spectrophotometer fitted with an integrating sphere, using $BaSO_4$ as the reference. Electron paramagnetic resonance (EPR) spectra were collected at room temperature in the X-band using a Bruker BioSpin E500 spectrometer. Electrochemical measurements were carried out in a conventional three-electrode configuration connected to an Ivium electrochemical workstation. Electrical measurements were performed using a Keithley 4200-SCS semiconductor parameter analyzer.

Calculation details. According to XRD and TEM results (Fig.S3 and S4), the as-prepared ZnO possesses a typical hexagonal wurtzite structure, predominantly growing along the [0001] direction (corresponding to the (002) planes serving as the terminating end facets) to form a one-dimensional

nanorod morphology, with the exposed surfaces mainly consisting of non-polar $\{10\bar{1}0\}$ facets on the side walls. In wurtzite ZnO, the (100), (010), and $\{10\bar{1}0\}$ facets are crystallographically equivalent non-polar planes, exhibiting nearly identical atomic arrangements and surface energy properties. Therefore, to simplify model construction while ensuring physical consistency, the (100) facet was selected as the representative surface to build the interface interaction model between ZnO and PQ$^{\bullet}$ molecules, aiming to elucidate the interfacial charge transfer mechanism. The Vienna Ab initio Simulation Package (VASP)[1–3] was employed to perform spin-polarized density functional theory (DFT) calculations. The generalized gradient approximation (GGA) with the Perdew–Burke–Ernzerhof (PBE) functional[4] was adopted to characterize the exchange–correlation interactions, while the projector augmented wave (PAW) method[5,6] was used to treat the electron–ion interactions. A plane-wave basis set was selected, with the cutoff energy set to 400 eV. For the bulk structure optimization of ZnO, a Monkhorst–Pack *k*-point mesh[7] with the configuration (10 × 10 × 6) was utilized. After optimization, the lattice parameters of wurtzite ZnO were determined as $a = b = 3.151$ Å, $c = 5.242$ Å (Fig. S6a), showing good consistency with the reported experimental data. For the three-layer ZnO (100) surface model (Fig. S6b), a (1 × 1 × 1) *k*-point mesh was adopted. To avoid interactions between adjacent periodic slabs, a vacuum layer of 15 Å in thickness was introduced. During the structural optimization of the ZnO (100) slab, the bottom atomic layer was constrained to its bulk lattice positions. For the PQ$^{\bullet}$@ZnO (100) (Fig. S6c), the structural optimization was performed with the bottom two atomic layers fixed. The convergence criteria for electronic relaxation were set as follows: the energy difference between consecutive iteration steps was less than 10^{-5} eV, and the Hellmann–Feynman force acting on each relaxable atom was within 0.03 eV/Å.

Electrochemical measurements. Mott–Schottky and Electrochemical Impedance Spectroscopy (EIS): Mott–Schottky and EIS Nyquist measurements were conducted in a standard three-electrode electrochemical cell using an Ivium electrochemical workstation. Working electrode preparation**:** 6 mg of the sample was dispersed in 2 mL of ethanol and sonicated for 15 minutes. 30 μL of the resulting suspension was then drop-cast onto a 1 × 1 cm^2 area of an ITO-coated glass substrate and dried at room temperature to form the working electrode. A three-electrode configuration was employed, with an Ag/AgCl electrode serving as the reference electrode and a Pt wire as the counter electrode. The electrolyte was a 0.5 M aqueous Na_2SO_4 solution (pH = 7).

Femtosecond transient absorption Measurements. TA measurements were performed using a Yb:KGW amplifier (Pharos, Light Conversion) coupled with a pump–probe spectrometer (HARPIA-TA, Light Conversion). The fundamental laser output (1030 nm, ~190 fs, 89 kHz) from the amplifier was divided into two beams. One beam was directed to an optical parametric amplifier (Orpheus, Light Conversion) together with a second harmonic generator (Lyra, Light Conversion) to produce a tunable pump pulse. The other portion of the 1030 nm beam was focused onto a sapphire crystal to generate a white-light continuum that served as the probe pulse. The pump and probe beams were spatially overlapped on the sample. The transmitted probe beam was dispersed by a monochromator (Andor Kymera 193i-B2) and detected with a silicon-based array detector. The pump–probe delay was controlled by a mechanical delay line with a maximum delay time of ns.

Light source. We used a series of semiconductor lasers for the UV–vis (375 nm: 3.95 mW cm^{-2}, 450 nm: 38.7 mW cm^{-2}, 520 nm: 32.2 mW cm^{-2}, 635 nm: 42.8 mW cm^{-2},730 nm: 15.4 mW cm^{-2},808 nm: 92.0 mW cm^{-2}) regions (Changchun New Industries Optoelectronics Tech Co., Ltd.) and a laser

power meter (with probe, CNI Laser. Changchun New Industries Optoelectronics Tech Co., Ltd.) to measure the photoresponsive behaviors of ZnO, $PQ^{\bullet}$@ZnO. The laser power and power density were calibrated using the power meter prior to measurements.

Supplementary Figures.

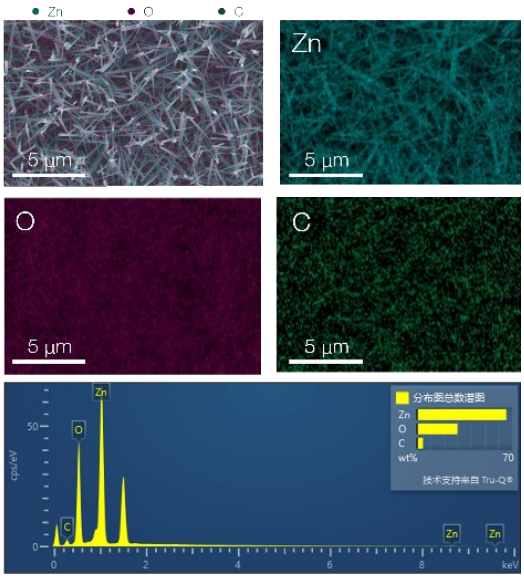

Fig. S1 SEM image, corresponding EDS elemental mapping of Zn, O, and C, and EDS spectrum of the PQ•@ZnO.

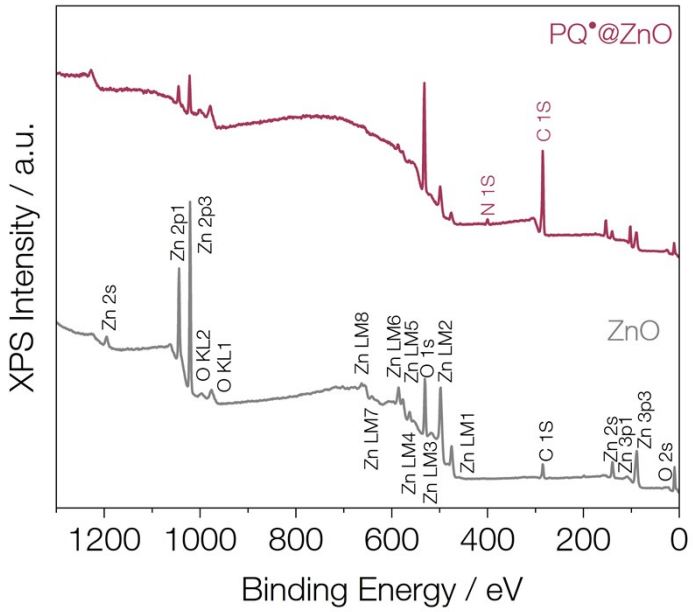

Fig. S2 XPS survey spectra of ZnO and PQ•@ZnO.

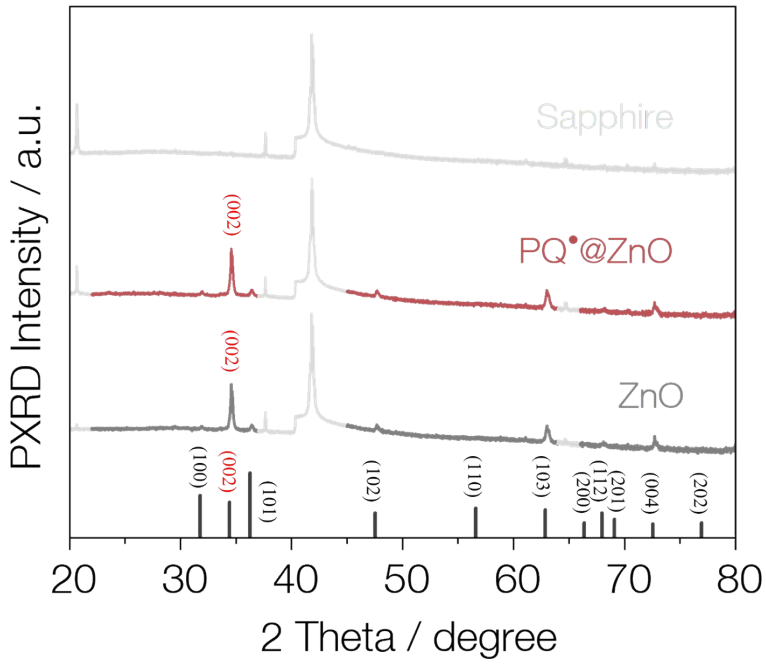

Fig. S3 PXRD patterns of ZnO and PQ•@ZnO.

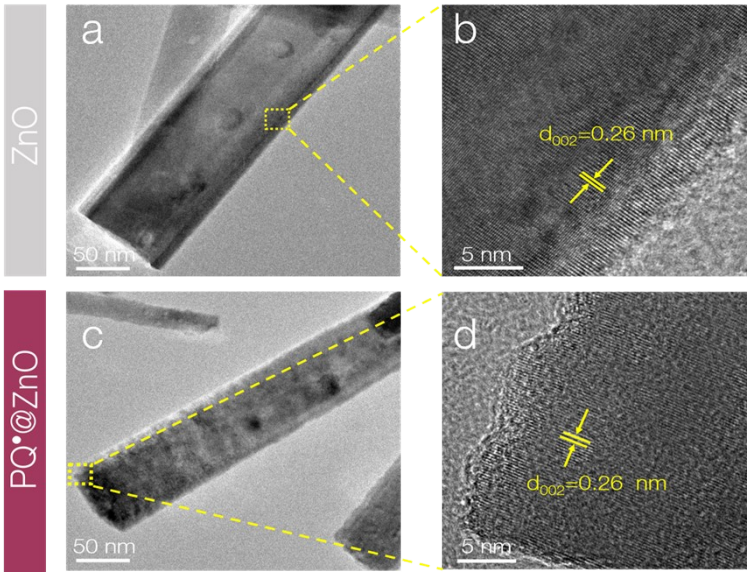

Fig. S4 Transmission electron microscopy (TEM) images and high-resolution lattice fringe characterizations of (a, b) ZnO and (c, d) PQ•@ZnO nanorods.

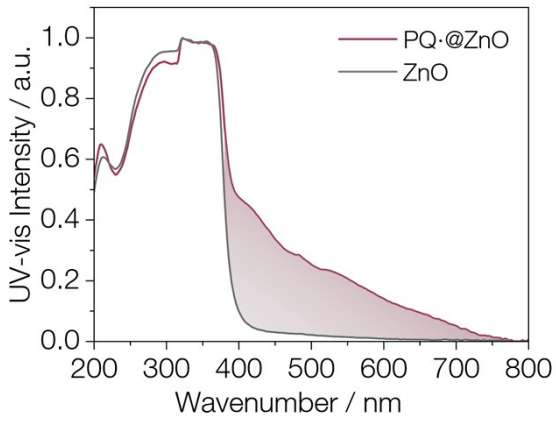

Fig. S5 UV–vis absorption spectra of ZnO and PQ•@ZnO.

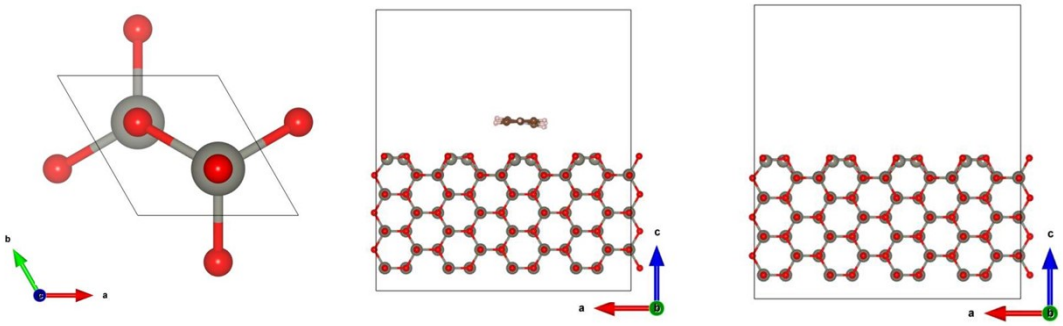

Fig. S6 Optimized structure for (a) ZnO primitive cell, (b) clean ZnO (100) slab, and (c) PQ•@ZnO (100) slab.

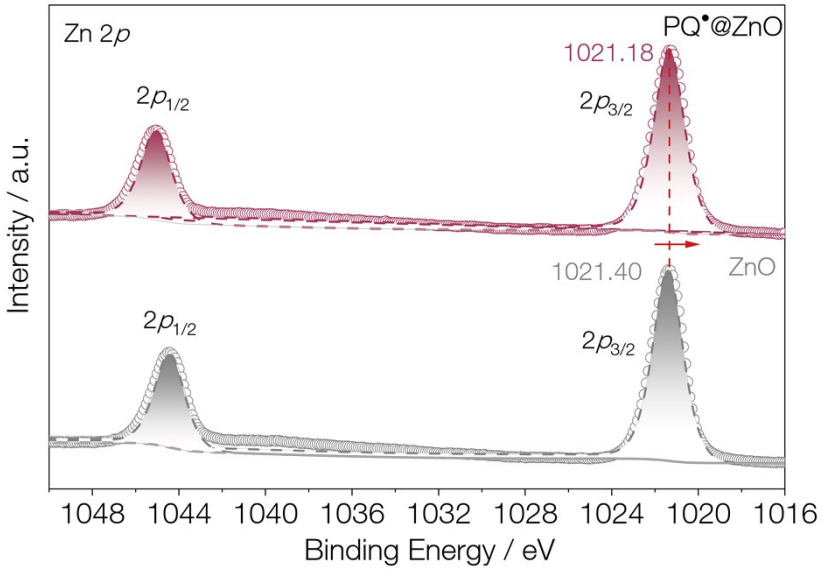

Fig. S7 High-resolution Zn 2*p* XPS spectra of ZnO and PQ•@ZnO.

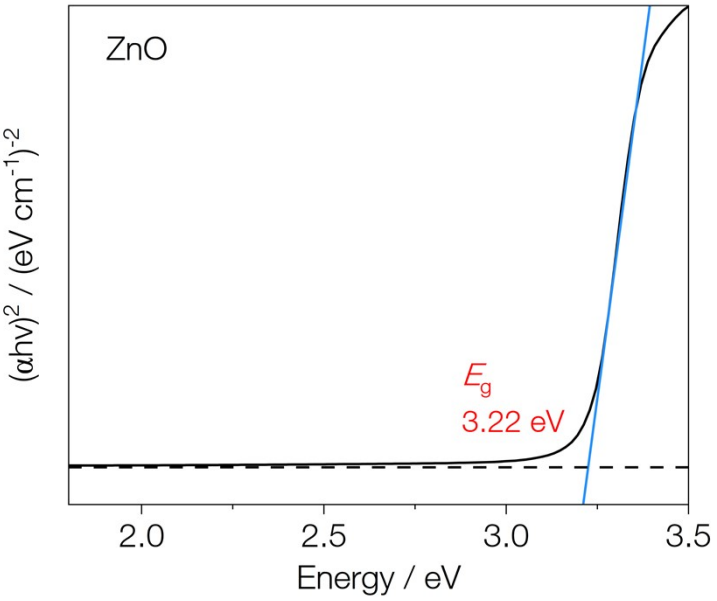

Fig. S8 Tauc plot of ZnO for bandgap determination.

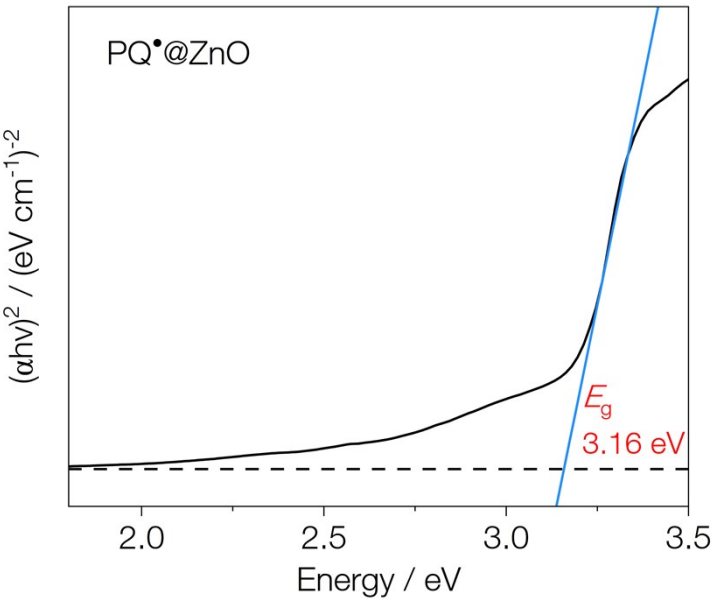

Fig. S9 Tauc plot of PQ•@ZnO for bandgap determination.

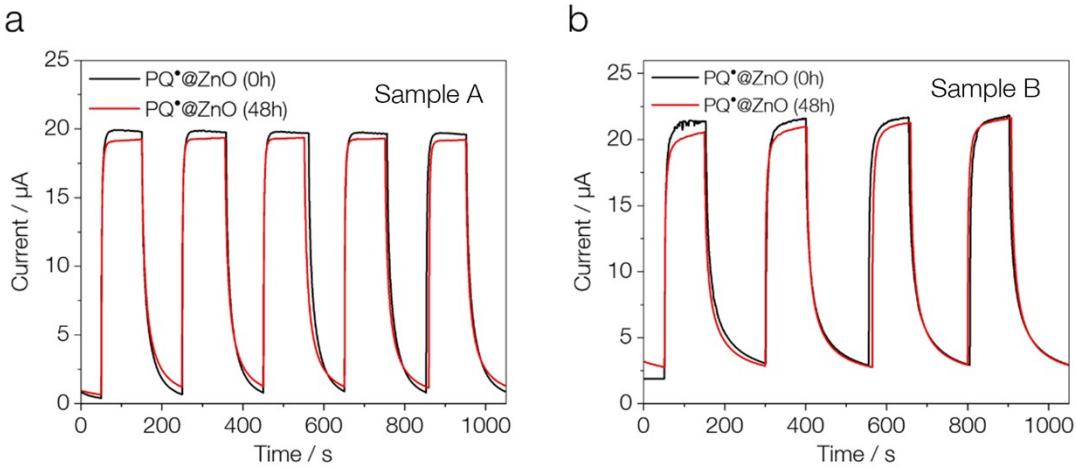

Fig.S10 *I–t* curves of samples A (a) and B (b) measured at 375 nm after exposure to air for 48 h.

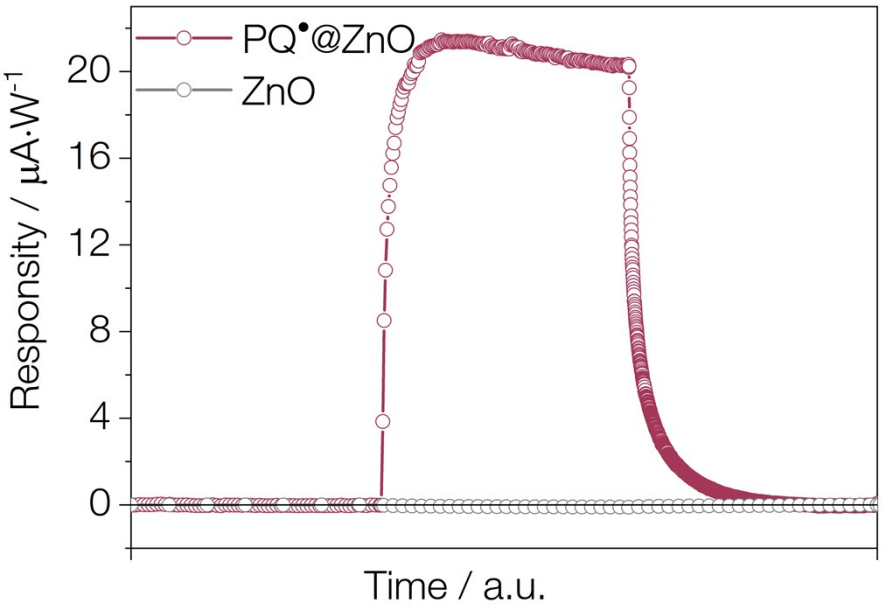

Fig. S11 Transient photo response curves of ZnO and PQ•@ZnO measured under 520 nm illumination at a bias voltage of 5 V.

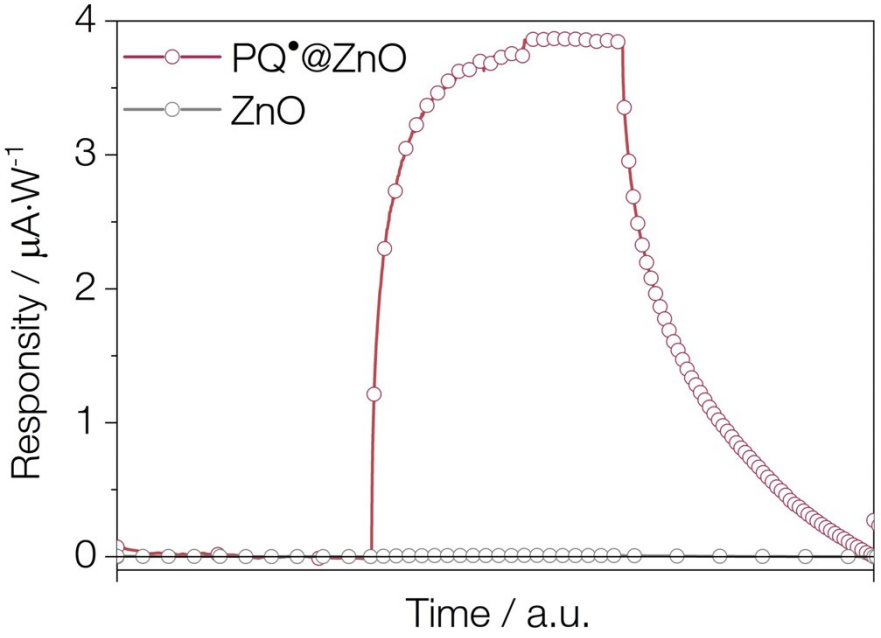

Fig. S12 Transient photo response curves of ZnO and PQ•@ZnO measured under 635 nm illumination at a bias voltage of 5 V.

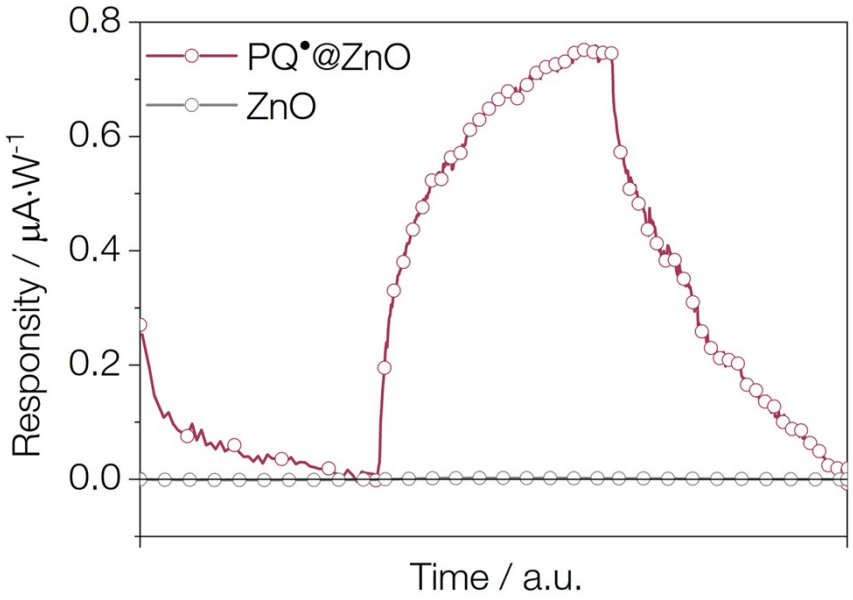

Fig. S13 Transient photo response curves of ZnO and PQ•@ZnO measured under 730 nm illumination at a bias voltage of 5 V.

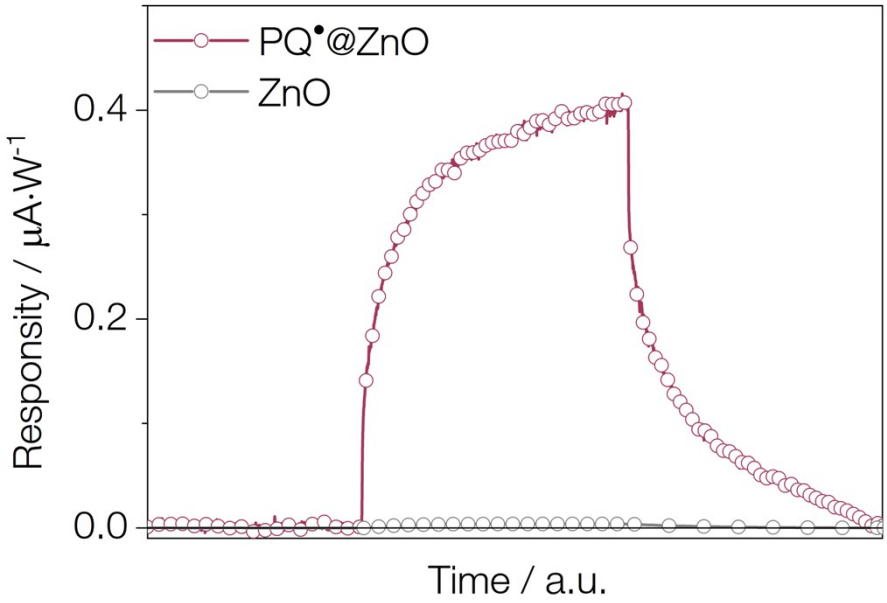

Fig. S14 Transient photo response curves of ZnO and PQ•@ZnO measured under 808 nm illumination at a bias voltage of 5 V.

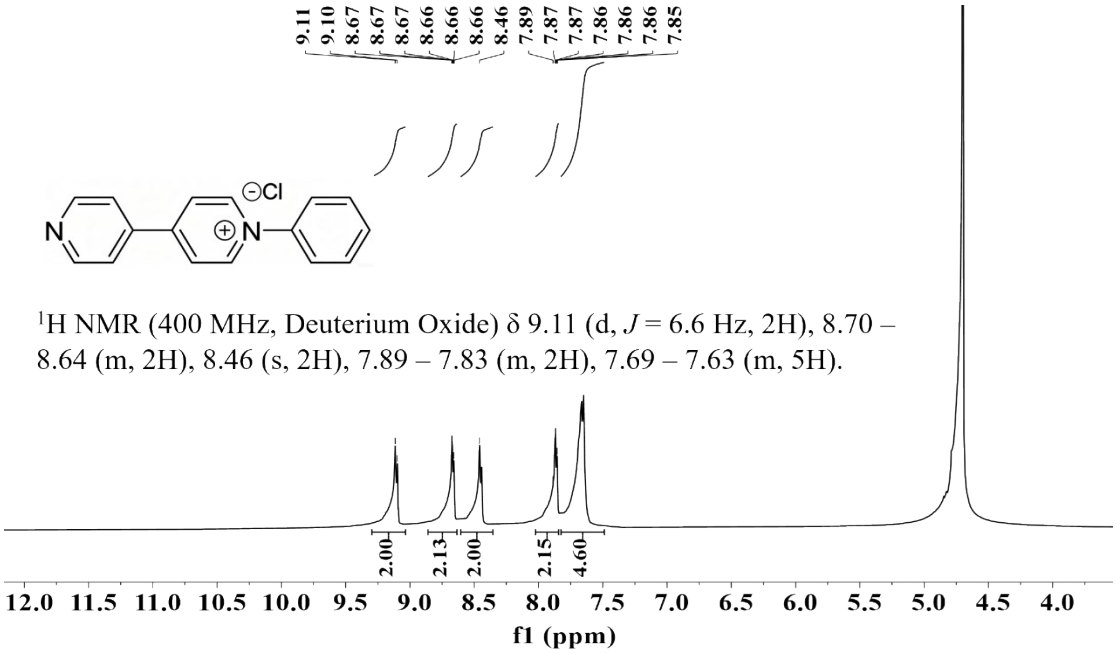

Fig.S15 [1]H NMR spectrum of the PQCl precursor recorded in D_2O

Table

Table S1 Responsivity comparison between pristine ZnO and PQ•@ZnO at different wavelengths.

Wavelength (nm)	ZnO (μA W^{-1})	PQ•@ZnO (μA W^{-1})	Enhancement (fold)
520	0.0825	20.80	252
635	0.00914	3.87	423
730	0.00239	0.71	297
808	0.00376	0.402	107

Table S2 Exponential fits for the *fs*-TAS decay of ZnO probed at 580 nm under 350 nm photoexcitation.

Sample	τ_1 (ps)	$-A_1$ (%)	τ_2 (ps)	$-A_2$ (%)	$\bar{\tau}$ (ps)
ZnO	2.97	56.51	22.90	41.33	19.9

The average lifetime ($\bar{\tau}$) can be calculated according to the following equation:

$$\bar{\tau} = -(A_1\tau_1+A_2\tau_2)/(A_1+A_2)$$

Table S3 Exponential fits for the fs-TAS decay of PQ•@ZnO probed at 580 nm under 350 nm photoexcitation.

Sample	τ_1 (ps)	$-A_1$ (%)	τ_2 (ps)	$-A_2$ (%)	τ_3 (ps)	A_3 (%)
PQ•@ZnO	5.77	41.9	23.0	36.6	201	21.5

REFERENCES

(1) Kresse, G.; Hafner, J. *Ab initio* molecular dynamics for liquid metals. *Phys. Rev. B* **1993**, *47* (1), 558–561.

(2) Kresse, G.; Furthmüller, J. Efficiency of ab-initio total energy calculations for metals and semiconductors using a plane-wave basis set. *Comput. Mater. Sci.* **1996**, *6* (1), 15–50.

(3) Kresse, G.; Furthmüller, J. Efficient iterative schemes for *ab initio* total-energy calculations using a plane-wave basis set. *Phys. Rev. B* **1996**, *54* (16), 11169–11186.

(4) Perdew, J. P.; Burke, K.; Ernzerhof, M. Generalized gradient approximation made simple. *Phys. Rev. Lett.* **1996**, *77* (18), 3865–3868.

(5) Kresse, G.; Joubert, D. From ultrasoft pseudopotentials to the projector augmented-wave method. *Phys. Rev. B* **1999**, *59* (3), 1758–1775.

(6) Blöchl, P. E. Projector augmented-wave method. *Phys. Rev. B* **1994**, *50* (24), 17953–17979.

(7) Monkhorst, H. J.; Pack, J. D. Special points for brillouin-zone integrations. *Phys. Rev. B* **1976**, *13* (12), 5188–5192.